City Research Online

City, University of London Institutional Repository

Investigation of a ground-cooled organic Rankine cycle for waste heat recovery

Montaser Mahmoud [a,b], Sumsun Naher [a], Mohamad Ramadan [c,d,*],
Mohammad Ali Abdelkareem [b,e], Hadi Jaber [f], Abdul-Ghani Olabi [b,g]

[a] Department of Engineering, School of Science and Technology, City, University of London, London, United Kingdom
[b] Sustainable Energy & Power Systems Research Centre, RISE, University of Sharjah, P.O. Box 27272, Sharjah, United Arab Emirates
[c] Lebanese International University, PO Box 146404 Beirut, Lebanon
[d] International University of Beirut, PO Box 146404 Beirut, Lebanon
[e] Chemical Engineering Department, Minia University, Elminia, Egypt
[f] Mechanical and Industrial Engineering Department, Abu Dhabi University, United Arab Emirates
[g] Mechanical Engineering and Design, Aston University, School of Engineering and Applied Science, Aston Triangle, Birmingham, B47ET, United Kingdom

ARTICLE INFO

ABSTRACT

This paper investigates a ground-cooled organic Rankine cycle (ORC) for waste heat recovery from a diesel generator. The ambient and ground temperatures used in the current study are based on real-time data collected from experimental measurements. ANSYS Mechanical APDL was used to simulate the effect of the proposed system on the ground in order to calculate the soil thermal interference radius. In addition, the simulation study compared two scenarios: with and without phase change material. Based on the simulation results, the required ground loop size was calculated using the Engineering Equation Solver (EES). The economic feasibility of the proposed system was investigated, considering both basic and regenerative ORCs. The original rated output power of the diesel generator considered in this study was 30 kW. The results showed that the soil thermal interference radius and the ground loop length were 0.32 m and 1480 m, respectively. The ORC system, with a design operating temperature of 300 °C, enhanced the overall output power by 7.98%, compared to that of diesel generator alone. Replacement of the basic ORC with a regenerative ORC increased the enhancement up to 15.31%. The capital cost and payback period ranges for the basic ORC were £11,945–18,770 and 4.9–7.8 years, respectively, while those for the regenerative ORC are £17,062–25,592 and 3.7–5.5 years.

1. Introduction

A huge amount of heat is wasted from industrial processes, engines, and power generation technologies. This elevates the importance of developing waste heat recovery (WHR) systems in order to employ this thermal energy instead of being wasted into the environment [1–3]. WHR systems can be used in various applications, including transportation [4], industrial processes [5], buildings [6], and power plants [7]. Endeavors have developed several WHR techniques aiming to fit each specific application based on the grade of wasted heat [8–10]. These systems can be found in the form of organic Rankine cycle [11], Kalina cycle [12], thermoelectric generator [13], regenerative burner [14], economizer [15], air preheater [16], heat pipe [17], and phase change material [18].

One of the most commonly employed WHR systems is the organic Rankine cycle (ORC), which uses an organic fluid instead of water compared to the conventional Rankine cycle. There are many applications that have been implemented that confirm the suitability of ORC in WHR applications [19–21]. The organic fluid has a lower boiling point than water, which allows it to evaporate at a lower temperature, making it suitable for use in low-temperature heat sources. The ORC can be used to generate electricity from various heat sources, such as geothermal energy [22], solar energy [23], waste heat from industrial processes [24], and biomass combustion [25]. The ORC works by using the heat from the heat source to evaporate the organic fluid, which then drives a turbine to produce electricity. ORC systems are also more efficient than traditional steam turbines at low temperatures, making them well-suited for use in renewable energy and low-grade WHR systems. There are

---

* Corresponding author.
  E-mail address: mohamad.ramadan@liu.edu.lb (M. Ramadan).

several types of ORCs available, including basic [26], reheated [27], transcritical [28], supercritical [29], dual pressure [30], dual fluid [31], and regenerative cycles [32].

One of the main problems facing ORCs is their low efficiency when the ambient temperature is high. This makes the expansion of the working fluid limited in the turbine, leading to a decrease in the output power and efficiency. This problem is also more significant when the heat source temperature is low, such as in various WHR systems. Another choice for cooling a power cycle is to use a cooling system to supply cold water to the condenser. However, this is still not a perfect replacement for the air-cooling system since it will consume additional amounts of power instead of being supplied. Thus, employing the ground as a cooling source is an attractive approach since it is more

stable and can provide cooling when the ambient air temperature is relatively high. On the other hand, there are only few reports that have investigated this approach, which represents a notable gap in research.

Vidhi et al. [33] employed the EAHE as a cooling device for low to medium-temperature power generation systems. The power cycle under investigation was the supercritical organic Rankine cycle, in which six organic fluids were compared: R32, R125, R134a, R143a, R170, and R218. The highest efficiency was achieved when using R134a as a working fluid. It was observed that the soil temperature surrounding the ground heat exchanger (GHE) pipes increased with the penetration depth. The results obtained showed that the incorporation of EAHE helped in increasing the power cycle by approximately 1% as well as reducing the daily power output fluctuations. A novel system with a
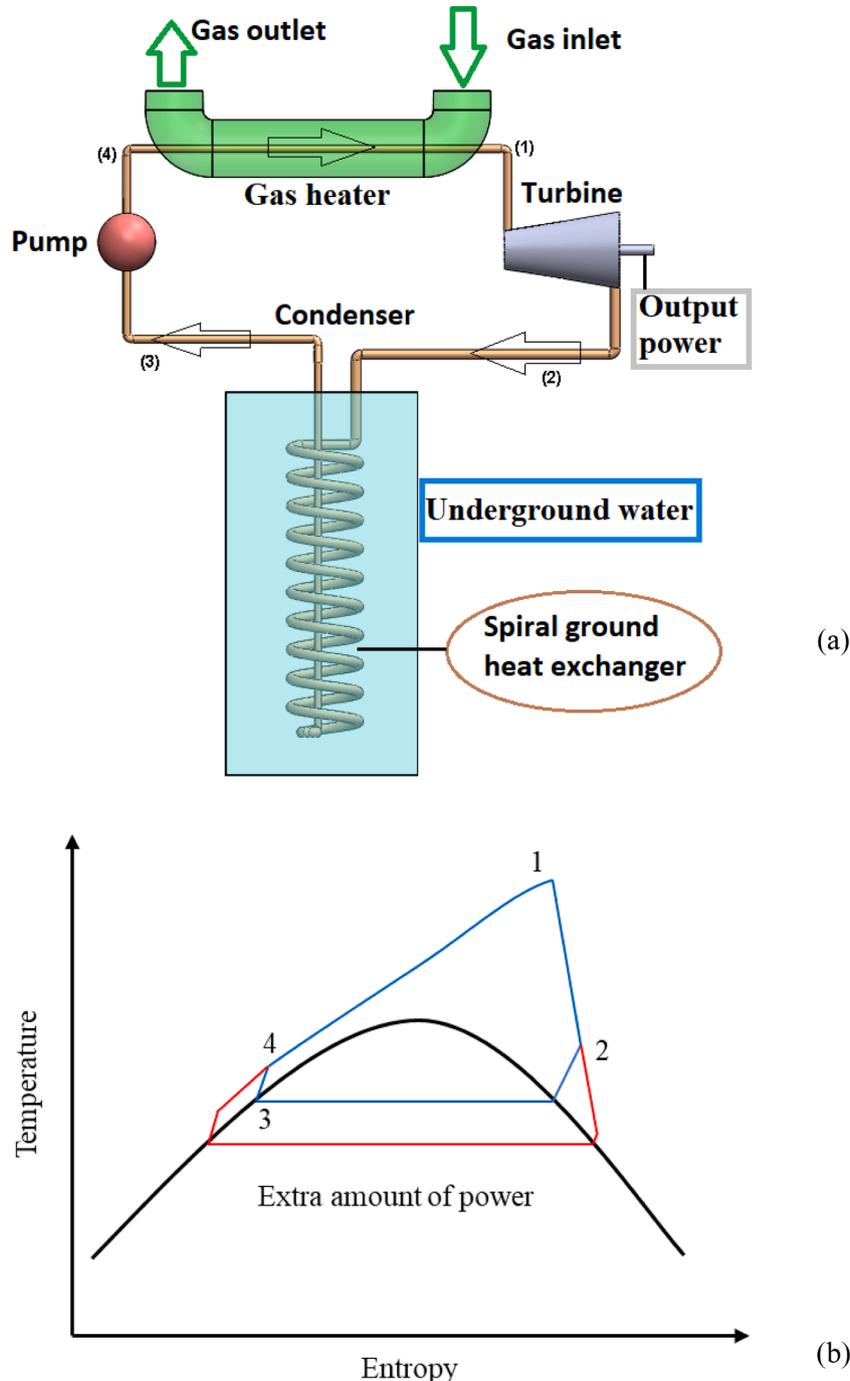
Fig. 1. (a) Schematic diagram of a ground-cooled organic Rankine cycle and (b) the adjusted T-S diagram [34]. (With permission number 5,511,401,153,610).

ground-cooled condenser and a CO_2-based transcritical Rankine cycle was presented in [34]. The gas temperature ranged from 500ºC to 1500ºC, and the mass flow rate ranged from 100 to 350 kg/hr. The investigation addressed a wide variety of conditions at the heat source. The study's objective was to optimize the cycle's net output power while taking into account the smallest possible heat exchanger. According to [35], at an expander inlet pressure of 3 MPa, the ground-cooled condenser can increase the cycle's net output power by 7.35%, 12.13%, and 8.77% for R123, R124, and R245fa, respectively. An experimental investigation on the utilization of a ground-cooled ORC was conducted by Mahmoud et al. [36]. The results showed that the indirect ground cooling system outperformed the direct system due to the significant pressure drop inside the ground loop. Additionally, it was reported that another heat rejector is required to support the GHE and avoid heat accumulation.

This research is a continuation of our previous studies that were published recently [34–36]. The current paper aims to investigate the effect of ground-cooled ORC on the ground temperature in order to estimate the soil thermal interference radius and calculate the ground loop size. The effect of the proposed cycle on the ground was first simulated in ANSYS Mechanical APDL, including a comparison between two cases: with and without phase change material (PCM). The soil thermal interference radius was then used to calculate the ground loop size using Engineering Equation Solver (EES). This software was also employed to compare the thermodynamic performance of the basic and regenerative cycles. Finally, a WHR application was taken as a case study in order to investigate the economic feasibility of the ground-cooled ORC.

2. Background

The purpose of employing a ground-cooled ORC is to improve the amount of energy produced by a power cycle, particularly in the summer when the ground temperature is essentially independent of the surrounding environment. As a result, when the ambient temperature is high during the summer, the GHE is a better alternative than the air heat exchanger. With the intention of creating favourable heat transfer conditions and facilitating the process of heat exchange with the aid of underground water, the geothermal condenser in [34] was installed in a well. Knowing that the source of heat discussed in [34] was the waste heat from an engine exhaust, Fig. 1 illustrates the proposed cycle, illustrating all its components. The amount of heat rejected from the cycle to the ground was not considered to affect the temperature of the subsurface water since it was regarded as remaining constant. This hypothesis may only be taken into account in one of two circumstances: either when the volume of the well is huge or when the ground-cooled condenser is acting as a supplementary condenser. The latter is strongly advised to provide stability since the primary condenser, which can be either air-cooled or water-cooled, can lessen the amount of heat that is rejected to the ground and make up for the coolth energy lost during off-periods. As WHR applications were the major focus of the proposed system's design, and since these applications often don't run continuously, ground/underground water can be employed as a cooling storage medium in this situation. As shown in Fig. 1a, a helical GHE condenser was chosen to reduce the overall GHE's volume. Fig. 1b shows the temperature-entropy diagram of the proposed cycle, displaying the enhancement in the cycle's net output power.

In [36], the GHE was placed in soil considering the absence of shallow underground water in many regions. A comparison between direct and indirect ground cooling systems was carried out with the aim of optimizing the output power and reducing the effect of critical parameters. The findings reported in [36] demonstrated that pressure drop's influence cannot be disregarded and would in fact have a major negative impact and alter the cycle's settings. So, it was advised to include an intermediary water loop between the cycle and the ground in order to assure stability, make the system easier to manage, and prevent serious problems caused by pressure losses. It is also crucial to note that,

as shown in [36], an antifreeze liquid must be combined with water in order to prevent freezing when the cooling source temperature falls below 0 °C.

In comparison to the shallow GHE capacity, the heat rejected from a power cycle can be substantial; otherwise, a larger installation would be necessary. As a result, the system becomes more expensive and is therefore inappropriate for certain applications. Thus, it is preferable to incorporate another heat rejector, such as an air-cooled or water-cooled heat exchanger, into the hybrid power cycle. The GHE receives cooling compensation as another benefit of this integration, which can significantly improve its performance during operation hours. The water loop will be operating throughout the night for this recovery system to function, transferring heat from the earth to the ambient air.

Fig. 2, which presents the optimal system proposed in [36], shows the two different types of heat exchangers connected in series. To prevent heat exchange with the ground when the surrounding air temperature is lower than the temperature of the ground, a shortcut link is connected in parallel with the GHE. The primary heat rejector, on the other hand, will constantly be in use to lessen the amount of heat that is transmitted to the ground from the cycle, reducing heat buildup and the requirement for substantial GHE installations. Due to this, a directional control valve (DCV) was installed at the primary heat rejector's output to regulate the water's flow route, allowing it to either pass through the GHE or bypass it entirely to enter the circulating pump. In order to bypass the cycle's condenser at night while the system is in recovery cooling mode, another DCV was installed at state 8. Consequently, by removing heat from the ground and transferring it to the surrounding air, the two bypass lines assist the earth in recovering its cooling energy by lowering its temperature while the power cycle is off. Moreover, a DCV must be used at the primary heat rejector's intake to aid the heat exchanger overtake when the water leaving the condenser is below ambient.

According to [35], a regenerator would be an interesting way to improve the thermodynamic efficiency of the cycle in the optimized system shown in Fig. 2, particularly when there is a significant temperature difference between states 2 and 4. Fig. 3 shows the regenerative cycle presented in [35], which intends to use the energy still present in the working fluid leaving the expander. On the other hand, it's important to determine whether this integration has any unfavourable effects, such as the quantity of heat that is rejected to the ground, which was addressed in [35].

3. System description

The schematic diagrams presented in Fig. 2 and Fig. 3 are both considered in the current study, which aims to compare their thermodynamic performance and cost effectiveness. This comparison will be based on the below design conditions and material properties that will be used to evaluate the soil thermal interference radius and ground loop size. In addition, another comparison will be conducted to determine if it is useful to incorporate phase change material (PCM) in this case or not. A schematic representation of the ground heat exchanger is presented in Fig. 4.

3.1. Design conditions

As presented in our previous study [36], there are three operating cases based on the ground and ambient temperatures. In this study, the first case is chosen to ascertain the design conditions since the ground cooling system is assumed to be operating 8 h/day. This corresponds to the maximum amount of heat injected into the ground in a day compared to the other two cases. The highest temperature reported at 2 m depth was 19 °C, which can be considered the initial temperature of the soil in the current simulations. The detailed variation of the ambient and ground temperatures in the current case study is presented in Fig. 5, which was collected experimentally. Taking a minimum temperature
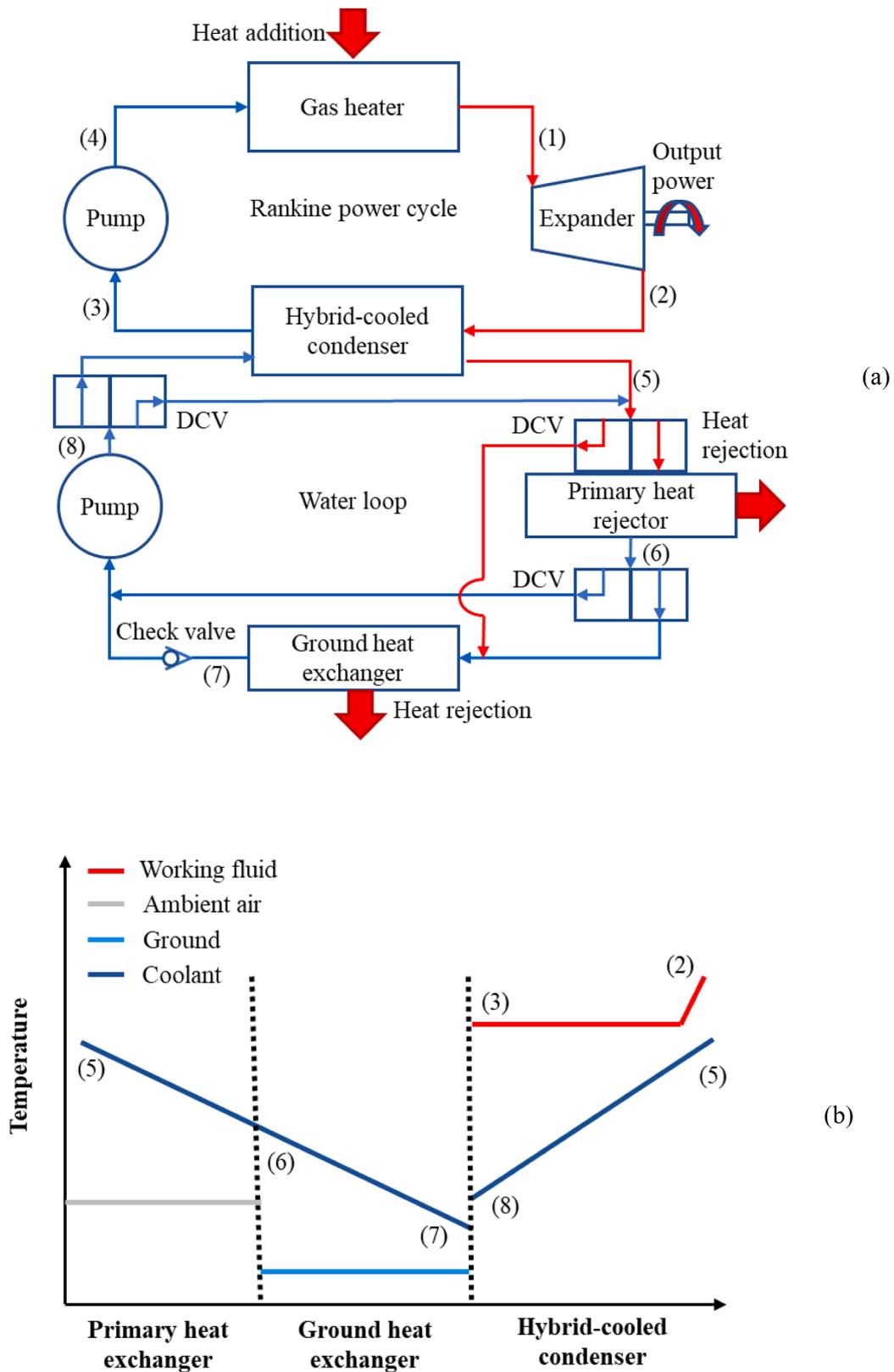
Fig. 2. (a) Schematic diagram of the optimized system and (b) temperature variation in the cooling system; directional control valve (DCV) [35,36]. (With permission numbers 5,511,401,358,421 and 5,511,410,203,697).

difference of 8 °C between the cooling source and working fluid, the condensation temperature can be assumed to be 27 °C. Thus, the water circulating through the GHE must have a temperature varying between 19 °C and 27 °C. Table 1 summarizes the design conditions needed for

the numerical simulations, and Fig. 6 presents the boundary conditions of the system.

The diesel generator's exhaust gas conditions presented in this paper are estimates and should be taken as average values due to the high
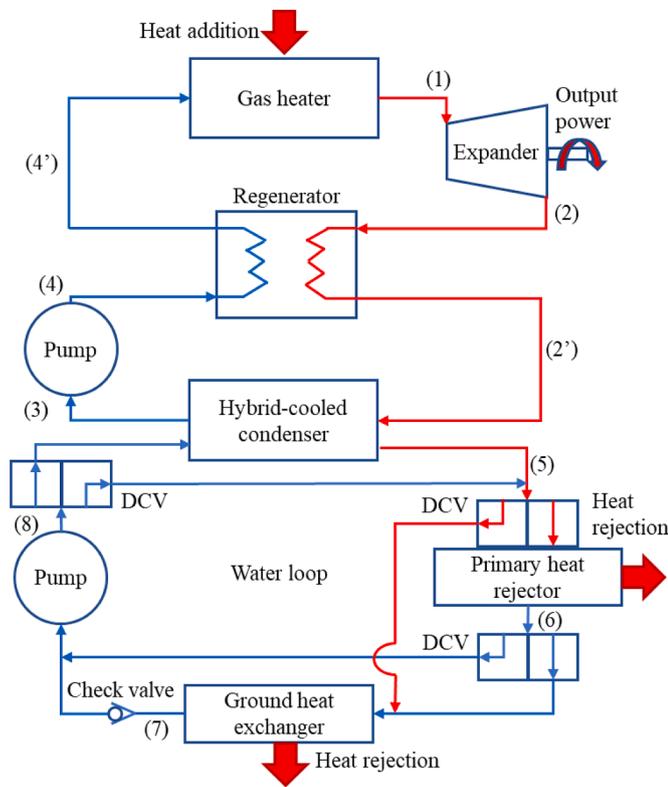
Fig. 3. Schematic diagram of the regenerative ground-cooled organic Rankine cycle [35]. (With permission number 5,511,410,203,697).
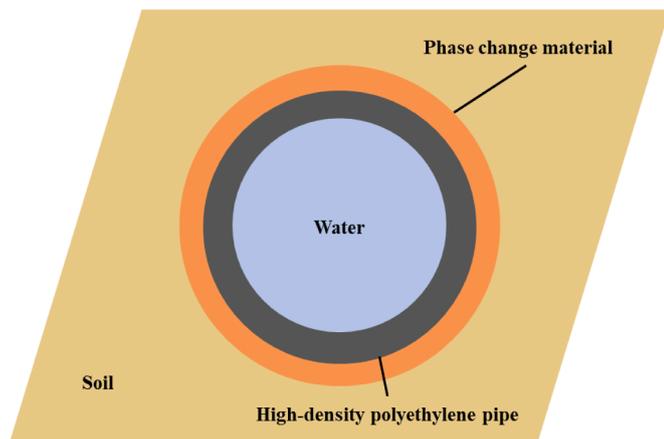
Fig. 4. Cross-sectional view of the ground heat exchanger with phase change material.

fluctuations in supply and demand. To avoid the effect of such significant variations, a diesel generator of 30 kW capacity with a diesel consumption of ~11 L/hr is investigated. This choice makes it easy to compare and compromise between the information provided by the manufacturer and the details reported by the generator's owner. The exhaust mass flow rate of gas can be estimated as 150 kg/hr, assuming an air to fuel ratio of 15. The specifications and design conditions of the diesel generator and ORC are presented in Table 2.

3.2. Material properties

The properties of soil, pipe, and phase change material are presented in Table 3. The values related to the soil are taken as averages since there are different types of soil. The inner and outer radii represent the

thickness of each material, such that the pipe and PCM have a thickness of 2.3 mm. However, the soil has two values for its inner radius considering the two investigated cases, with and without PCM. Rubitherm (RT 21HC) is used as the latent storage material since its melting/solidification temperature is between the highest and lowest temperatures of the fluid circulating through the pipes. It has a latent heat of 190 kJ/kg and densities of 770 and 880 kg/m^3 for the liquid and solid phases, respectively. The specific heat of both phases is approximated as 2 kJ/m. °C; however, during the change of phase, it varies significantly. This rise in its specific heat represents the latent heat of fusion in the ANSYS software. RT 21HC also has an advantage in the sensible storage since its specific heat in both phases is higher than that of soil and high-density polyethylene (HDPE). The corresponding values of the latter materials are 0.8 and 1.865 kJ/m. °C.

4. Methodology

In this study, two software tools are used: ANSYS and EES. The former is used to simulate the thermal response of the ground in order to calculate the soil thermal interference radius. The data collected from ANSYS will then be introduced to the EES model to evaluate the size of the ground loop. A stress analysis was also conducted in EES to ensure that the pressure inside the pipes is not exceeding the allowable stress. Additionally, EES was also used to compare the thermodynamic performance of the basic and regenerative cycles based on the WHR application that will be presented below.

4.1. ANSYS

The simulations were carried out using ANSYS software to investigate the thermal distribution. This software has been selected since it is simple, robust, available, and cheap. The study covers a circular area with a radius of 0.6 m since it is expected that the thermal interference will not exceed this radius and the results will be more precise and reliable. The areas created in ANSYS represent different materials; three areas were created in the case of using phase change materials: soil, pipe, and RT 21HC. However, only two areas were created in the other case when the phase change material was not added. The inner and outer radii of each area are taken as presented in Table 3. The procedure used to conduct the simulations on ANSYS is presented below:

Preferences: Thermal

Preprocessor:

- Element type → Solid Quad 3node 55
- Material properties → Material models (Thermal conductivity, density, and specific heat)
- Modelling:
  ○ Create → Areas → Circle → Annulus
  ○ Operate → Booleans → Glue → Areas
- Meshing:
  ○ Mesh attributes
  ○ Size controls
  ○ Mesh

Solution:

- Analysis:
  ○ New analysis → Transient
  ○ Solution Controls: Enter the time of load step and number of sub steps
- Define loads → Apply:
  ○ Thermal: Convection
  ○ Initial Condition: Enter the initial temperature
- Solve

General postprocessor: Plot and list the results
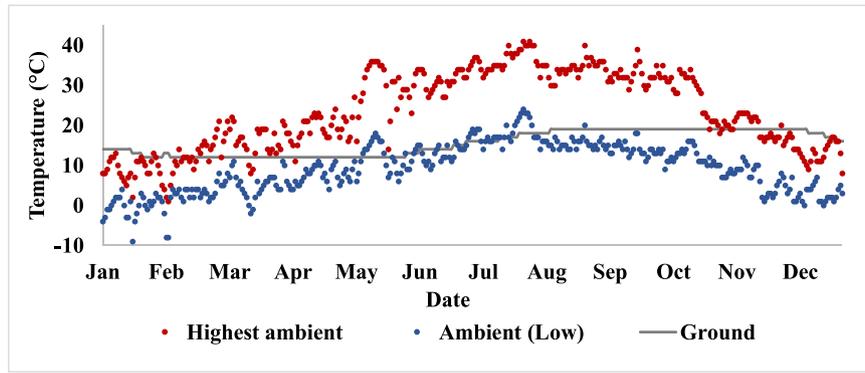
Fig. 5. Comparison between the ambient and ground temperatures in Lebanon during 2020 (experimental measurements).

Table 1
The design conditions for ANSYS simulations.

Parameters	Values	Units
Initial ground temperature	1 9	°C
Water inlet temperature	2 5	°C
Water outlet temperature	2 1	°C
Water mass flow rate	0.85	kg/s
Specific heat of water	4.18	kJ/kg.K
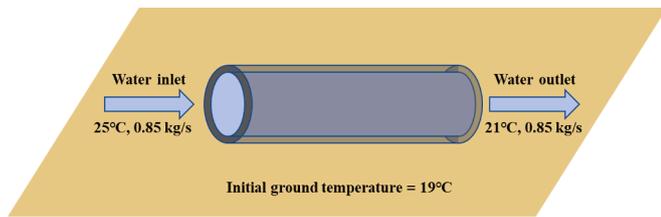
Fig. 6. Boundary conditions.

Table 2
The design conditions of organic Rankine cycle and exhaust gas of diesel generator.

Parameters	Values	Units
Gas mass flow rate	150	kg/hr
Gas inlet temperature	5 00	°C
Gas exit temperature	1 00	°C
Diesel generator capacity	30	kW
ORC working fluid	R123	–
Expander inlet pressure	5	MPa
Expander isentropic efficiency	70	%
Pump isentropic efficiency	90	%
ORC generator efficiency	90	%

Table 3
The properties of the materials considered for the current simulations [37–39].

Materials	Soil	High-density polyethylene pipe	Phase change material (RT 21HC)
Thermal conductivity (W/m.K)	2	0.5	0.2
Density (kg/m^3)	1500	953	770–880
Specific heat (kJ/m.°C)	0.8	1.865	2
Latent heat (kJ/kg)	–	–	190
Inner radius (mm)	34.3–36.6	32	34.3
Outer radius (mm)	600	34.3	36.6

4.1.1. Meshing

The materials used in this study were created using the Solid (Quad 4node 55) as the thermal element type. These were all modelled as areas in which they were glued, allowing the user to use different types of material properties. The created meshes are almost the same in both cases (with and without PCM) due to the large relative radius of the area under study compared to that of PCM and HDPE (see Fig. 7). The size of elements was kept as the default since it is found to be suitable for the accuracy of thermal distribution (small elements near the centre). The size of elements created at the peripheries is not a constraint because the soil thermal interference radius will not spread to reach these elements.

4.1.2. Sensitivity analysis

As mentioned previously (section 4.1.1), the size of the element edge was set by the software automatically (the default size). On the other hand, similar results could be obtained if the size is added manually by the user. Thus, a sensitivity analysis based on the size of meshing was done to determine the maximum acceptable element edge length and avoid high computational durations. In this particular case, the convergence criteria method was used to determine the maximum acceptable element edge length for a sensitivity analysis based on mesh size. By varying the size of the meshing elements and examining the resulting nodal thermal distribution, the analysis seeks to identify the element edge length that produces stable, reliable results without excessive computational time. The sensitivity analysis was carried out by comparing the nodal thermal distribution after 8 h of operation. At first, the size of the element's edge was taken as 150 mm. It was noticed that the results are not acceptable for the cases where the element edge size is greater than 75 mm since the soil thermal interference radius was not steady. At 75 mm, the soil thermal interference radius was almost clear and agreed well with the simulation results of 50 mm and those of section 5.1. However, it does not provide detailed results regarding the thermal distribution in the HDPE pipe, where the inner edge of the pipe is presented as a square. Thus, the size of the element edge must not exceed 50 mm, where the results are steady and provide a detailed and clear image of the thermal distribution and soil thermal interference radius.

4.2. Engineering equation solver (EES)

As this research is part of a continuation study, only the additional equations required to complete the current modelling are provided in this section. As a result, it is advised to refer to the previously mentioned studies for further illustration of the developed model [34–36]. According to the theory of modelling presented in [34], the convection heat transfer coefficient depends significantly on the mass flow rate of the circulating fluid. The following equation can be used to evaluate the mass flow rate of water:
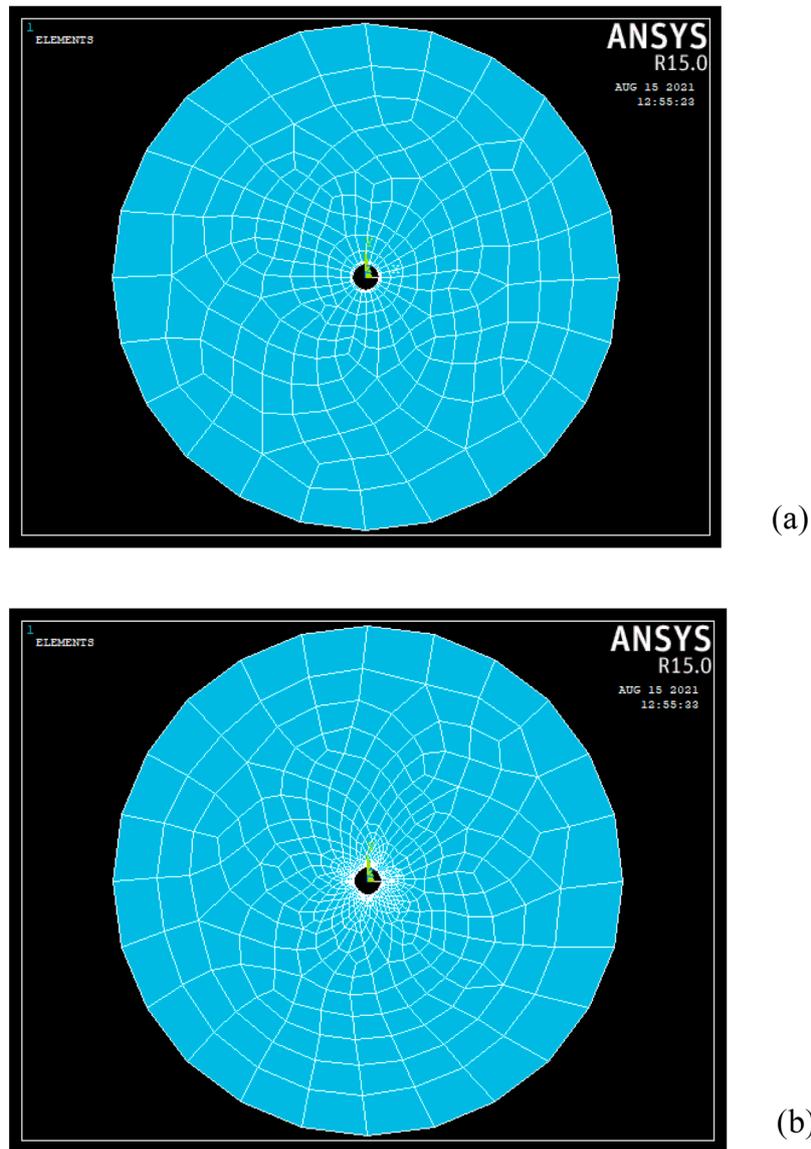
Fig. 7. The meshing of areas in ANSYS (a) with and (b) without phase change materials.

$$\dot{Q}_{rej} = \dot{m}_w c_{pw} \Delta T_w \tag{1}$$

where $\dot{m}_w$ is the mass flow rate of water, c_{pw} is the specific heat and ΔT_w is the temperature difference of water.

Three resistances are considered in the calculation of ground loop size that correspond to the convection between the coolant and pipe, conduction in the HDPE pipe, and conduction in the soil. The following equation can be used to calculate the size of the ground loop based on the value of heat rejected computed using Eq. (1):

$$\dot{Q}_{rej} = \frac{\Delta T_{lm}}{R_{eq}} \tag{2}$$

where $\dot{Q}_{rej}$ is the heat rejected from the coolant, ΔT_{lm} is the log mean temperature difference and R_{eq} is the equivalent resistance of the three materials considered.

The equation used for the calculation of net output power in [34,35] has been adjusted in this section to include the effect of the GHE's length and water pump. Eq. (3) shows the adjusted form for the calculation of net output power.

$$\dot{W}_{net} = \dot{W}_t \eta_g - \dot{W}_{po} - \dot{W}_{pw} \tag{3}$$

where $\dot{W}_{net}$ is the net output power, $\dot{W}_{po}$ is the power consumed by the ORC pump, and $\dot{W}_{pw}$ is the power consumed by the water pump. The latter depends mainly on the length of the GHE and mass flow rate of circulating water. The following equation can be used to evaluate the amount of power consumed by the water pump:

$$\dot{W}_{pw} = \Delta P . Q \tag{4}$$

where ΔP is the pressure drop, as evaluated by Mahmoud et al. [36], and Q is the volumetric flow rate of water.

One of the most important studies that needs to be considered is the assessment of the heat exchanger's mechanical design. Based on the American Society of Mechanical Engineers (ASME), the minimum required thickness of the pipe can be calculated using the following equation [40]:

$$thickness = \frac{pr}{\sigma} \tag{5}$$

where p is the internal pressure, r is the inner radius, and σ is the maximum allowable tensile stress.

5. Results and discussion

5.1. Simulation results

The first run of simulations was carried out in the absence of latent storage material. Based on the nodal thermal distribution analysis, the temperature at the boundaries of the pipe immediately increased to reach approximately the same temperature as the circulating fluid (25 °C) after one hour (see Fig. 8). However, the soil thermal interference radius increases slowly with time, reaching a value of ~0.32 m after 8 h, which is the maximum operating duration. This means that the distance between the horizontal pipes must be equal to or greater than 0.64 m to avoid heat accumulation.

The second run of simulations was carried out considering the insertion of RT 21HC as a PCM around the HDPE pipe. Based on the contour plot of temperature distribution, it can be noticed that the soil thermal interference radius (~0.32 m) is insignificantly affected by the incorporation of PCM (see Fig. 9, Fig. 9). However, high temperatures were more confined to the centre in this case. Additionally, the temperature near the pipe is lower than that without PCM at all instants, revealing the effect of PCM's melting during the charging process.

5.2. Ground loop sizing

The length of the GHE will be calculated in the case where no PCM is used. This is mainly due to the insignificant effect of PCM on the soil thermal interference radius and the high capital cost of PCM incorporation. As reported in previous studies, the material surrounding the GHE has a significant effect on the system's performance [41–45]. Thus, it would be recommended to investigate modern types of PCM in future studies that may further enhance the thermal performance of the GHE, such as nano-enhanced [46–49], foam-based [50–52], bio-based [53–55], micro-encapsulated [56–58], and macro-encapsulated PCM [59–61]. To estimate the length of the GHE, the exhaust gas of a diesel generator is taken as the source of energy, which will be presented completely in the next section. The flue gas has a constant mass flow rate and temperature of 150 kg/hr and 500 °C, respectively. The selected working fluid is R123 based on the analysis presented in [35], and the heat added to the cycle is evaluated as 17.72 kW when the expander inlet temperature is fixed at 300 °C. At these values, the heat rejected from the cycle varies between 14.13 and 14.58 kW depending on the cooling source temperature, with an average value of 14.45 kW. Based on Eq. (2), the length of GHE can be calculated as 1423 m for the basic ORC and the regenerative cycle, considering the same expander inlet temperature. However, if the temperature increases to match the optimal operating conditions of the regenerative cycle [35], the length

will also increase, albeit insignificantly, to a value of 1480 m. This is the case for the regenerative cycle when it is running at its highest performance. The increase in size is mainly due to the rise in the amount of heat rejected from the cycle, which will increase from 14.45 to 15.72 kW. Table 4 summarizes the results obtained from the conducted simulations.

5.3. Case study

This section aims to present a real-world application on the use of the proposed technology (hybrid cooling system). This will be based on the results and analyses of our previous studies that investigated ground temperature variation [36] and working fluid selection [35]. In Lebanon, electricity outages are a common problem that occur daily. For this reason, the private sector managed to overcome this problem by providing electricity via diesel engine generators. The capacities of these generators are usually very small, avoiding high capital costs. Here comes another problem, which is the low efficiency of the old generators that are mostly used. The proposed system presented in the current paper suits well such an application which can be used as a WHR system to provide an additional amount of power. This can be easily adopted in rural areas such as Bekaa, where there are enough spaces for installing horizontal GHEs. In Bekaa, the maximum operating duration of diesel generators is 8 h/day, but this is randomly distributed between 06:00 and 24:00. The upcoming sections will present the contribution of the ground cooling system to reducing fuel consumption and increasing the net output power.

5.3.1. Stress analysis

As shown in Table 2, the highest pressure in the cycle is 5 MPa, which is the pressure inside the gas heater. It is recommended to use copper pipes for the ORC since they have a very high thermal conductivity. The maximum allowable tensile stress for copper is 90 MPa. Based on the previous sections, the inner radius varied between 0.005 and 0.01 m. Thus, according to Eq. (5), the minimum required thickness can be calculated as 0.278 and 0.556 mm, respectively. These correspond to outer diameters of 10.56 and 21.11 mm.

5.3.2. Optimal operation

As reported in [35], each working fluid has an optimal expander inlet temperature at a given pressure. Thus, it is essential to first find this temperature before installation to achieve the highest possible performance. Fig. 10 shows the variation of net output power for R123 while varying the expander inlet temperature. This result was obtained at an expander inlet pressure of 5 MPa and a condensation temperature of 18 °C. It can be noticed that the maximum net output power is
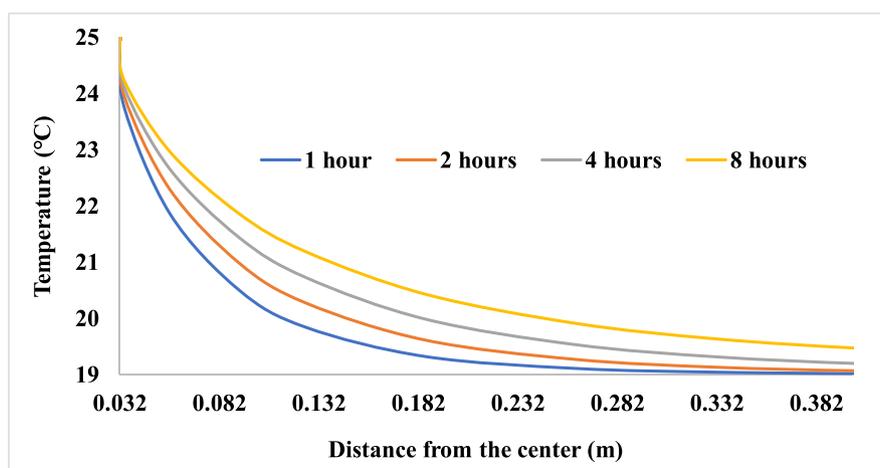
Fig. 8. The thermal distribution in soil without using phase change material during 8 h of operation.
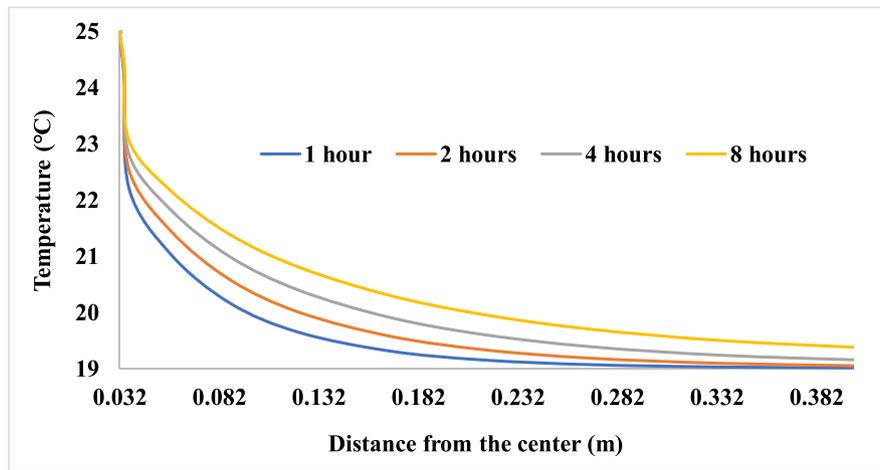
Fig. 9. The thermal distribution in soil using RT 21HC as a phase change material.

Table 4

Summary of the results obtained from ANSYS simulations and analytical calculations for ground loop sizing.

Parameters	Values
Maximum operating duration	8 h
Soil thermal interference radius	~0.32 m
Heat rejected from the cycle	14.45 – 15.72 kW
Ground loop length	1480 m
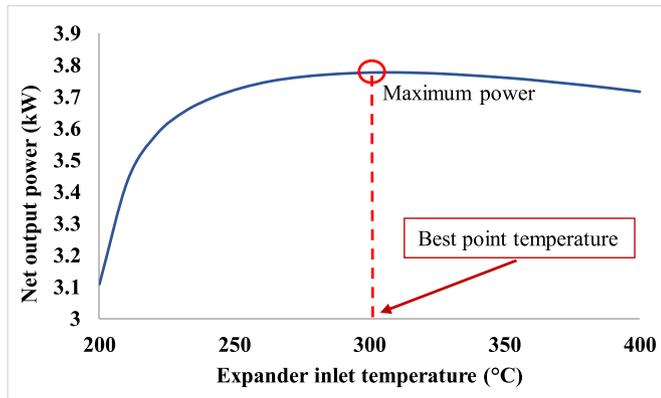
Fig. 10. The variation of net output power as function of expander inlet temperature for R123 at 5 MPa.

approximately 3.8 kW, which was achieved at an expander inlet temperature of ~300 °C. For this reason, the expander inlet conditions will be fixed in the upcoming sections. However, the other cycle's conditions will vary based on the cooling source temperature, which is assumed to fluctuate daily.

On the other hand, if the regenerative cycle is to be adopted, the best point temperature will change since the net output power of the cycle will be directly proportional to the expander inlet temperature [35]. However, to make a good comparison between the basic and regenerative ORC, the same conditions as the basic ORC with an expander inlet temperature of 300 °C will be considered.

5.3.3. Thermodynamic performance

According to calculations and simulations carried out in the previous studies [34–36], the mass flow rate of water can be approximated as 0.85 kg/s and the length of the GHE can vary between 1423 and 1480 m. Thus, the amount of power consumed by the water pump could be

estimated as 0.55 kW for the basic and regenerative ORC at an expander inlet temperature of 300 °C.

The daily average effective cooling source temperature varies based on the ambient air and ground temperatures, as shown in [36]. Assuming a constant temperature difference (8 °C) between the cooling source and condensation temperatures, both should vary similarly. According to this variation, the daily ORC net output power has been calculated and presented in Fig. 11.

The average power generated by the ORC is 2.395 kW, which corresponds to an enhancement of 7.98%. This means that the owner can increase the supply capacity from 30 kW to 32.395 kW. The second method that could be used is to fix the generator's capacity at 30 kW and reduce the diesel consumption. However, the first method would be better considering the difference between the levelized cost of electricity and fuel consumption cost per unit of energy. The overall system's efficiency varies between 12.89% and 15%, with an average value of 13.52% (see Table 5). The total energy generated per year from the ORC is approximately 7011 kWh.

Based on the same model used in the previous section, the net output power for the regenerative cycle can be evaluated at two different expander inlet temperatures (see Fig. 12). A considerable extra amount of power can be generated if the expander inlet temperature increased, as reported in [35]. However, this may be accompanied by a significant increase in the capital cost which will be discussed in the next section.

The average power of the regenerative cycle is significantly higher than that of the basic ORC, with an enhancement of 15.31% compared to the original power supplied by the diesel engine generator (30 kW). This value corresponds to the regenerative cycle running at an expander inlet temperature of 300 °C. Table 6 summarizes the regenerative cycle's
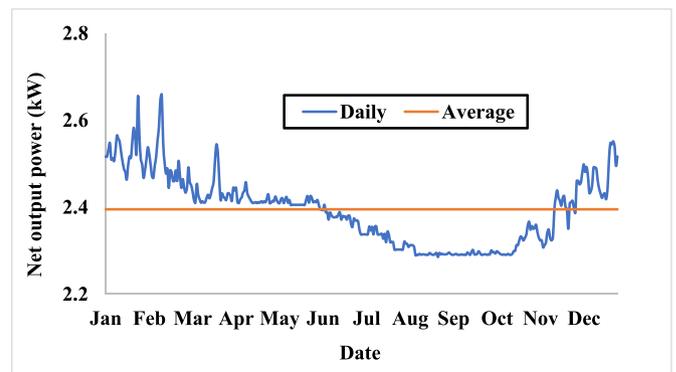
Fig. 11. The annual energy generated by the organic Rankine cycle.

Table 5
The performance of organic Rankine cycle; power and efficiency.

Performance	Minimum	Maximum	Average
Net output power (kW)	2.285	2.658	2.395
Efficiency (%)	12.89	15	13.52
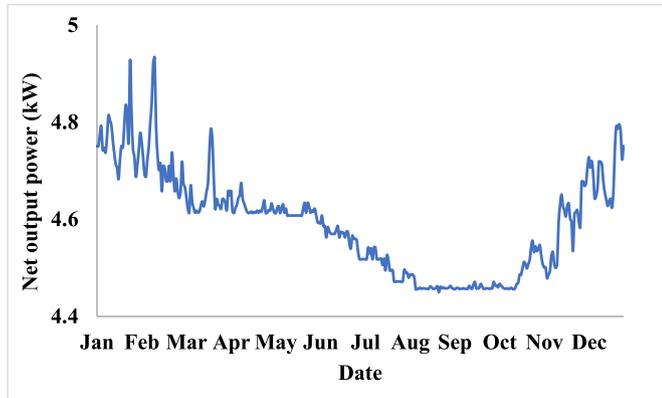
Fig. 12. The annual energy generated by the regenerative organic Rankine cycle.

Table 6
The performance of the regenerative organic Rankine cycle.

Performance	Minimum	Maximum	Average
Net output power (kW)	4.449	4.932	4.592
Power enhancement (%)	14.83	16.44	15.31

performance with respect to its net output power and power enhancement compared to the basic power generated by the diesel generator (30 kW). If the system operates 8 h/day, the annual energy generated by the regenerative ORC could be estimated as 13,447 kWh at expander inlet temperatures of 300 °C.

5.3.4. Cost analysis

The levelized cost of electricity supplied by the private sector (£0.35/kWh) is approximately twice that of the government. This makes the use of WHR system highly attractive since it is expected to have an acceptable payback period. The operating cost of diesel generator is calculated as £0.188/kWh since the cost of diesel in Lebanon is £0.5/L and the fuel consumption per unit of energy is 0.37 L/kWh. Concerning the capital cost, it can be divided into three main parts that are the ORC, groundwork and GHE pipes. The groundwork has been presented as a range based on the shallow geothermal conditions, however the cost of ground loop depends on the diameter, thickness and material used. High density polyethylene is selected in this case with a 32 mm diameter for several reasons: corrosion resistance, durability, resistance to pressure, easy mounting, and low friction. Table 7 presents all details required for estimating the capital and operating costs.

According to the same levelized cost of electricity (£0.35/kWh), the

Table 7
The average cost of system's components and operation.

Component/operation	Cost
Organic Rankine cycle (£/kW) [62]	2250–3000
Diesel consumption (L/kWh)	0.37
Levelized cost of electricity (£/kWh)	0.35
Diesel cost (£/L)	0.50
Operating cost (£/kWh)	0.188
High density polyethylene - 32 mm inner diameter (£/m)	1.25
Groundwork (£/m)	2.07–5.18

entire plant becomes more profitable when the operating cost decreases from £0.188/kWh to £0.173/kWh while using the proposed system. This is due to the extra amount of power produced for the same diesel consumption per hour. However, the diesel consumption per unit of energy is also reduced, from 0.37 to 0.34 L/kWh. The detailed cost assessment of the proposed system is presented in Table 8, in which the capital and operating costs are £11,945–18,770 and £0.173/kWh, respectively. As mentioned previously, the proposed system is expected to work 8 h/day at a rated average power of 2.395 kW. This means that the total gain can be estimated as £2419/year considering the levelized cost of electricity as £0.35/kWh. Thus, the payback period of the system is expected to be between 4.9 and 7.8 years, depending on three main factors: the operating hours, diesel generator load operation, and shallow geothermal conditions.

Considering the adoption of the regenerative cycle running at an expander inlet temperature of 300 °C, it can be noticed that the capital cost of the system is approximately 1.4 times greater than that of the basic ORC (see Table 9). On the other hand, the payback period decreases significantly in the case of the regenerative cycle, in which it has an average value of 4.6 years. This makes the regenerative cycle more attractive than the basic ORC since the latter has a minimum expected payback period of 6.4 years. This is due to the drop in operating cost, which decreased from 0.173 to £0.165/kWh. Therefore, the regenerative cycle is more preferable, as it has an annual net profit of £4640, which is considerably higher than that of the basic cycle (£2419).

6. Conclusions

This paper presented an investigation on a ground-cooled ORC aiming to calculate the soil thermal interference radius, ground loop size, capital cost, operating cost, and payback period. This investigation contributes to the field by providing a comprehensive analysis of the mentioned system, which can be useful for researchers and practitioners working in this area to design more efficient and effective GHEs, optimize ground loop systems, compare different scenarios to reduce capital and operating costs, and determine the limitations and feasibility of using ground-cooled ORC systems. The soil thermal interference radius is one of the most crucial parameters related to GHEs. It depends mainly on the amount of heat rejected to the ground, mass flow rate, operating duration, fluid temperature, and initial ground temperature. In the proposed system, the heat rejected to the ground was evaluated as 14.45–15.72 kW. Under the investigated conditions, the soil thermal interference radius was estimated using ANSYS and found to be approximately 0.32 m, considering a maximum operating duration of 8 h/day. Based on this finding, the length of the ground loop was calculated using EES, with a corresponding value of 1480 m. The proposed system was applied as a waste heat recovery system on the exhaust of a diesel generator with a capacity of 30 kW. Based on the design conditions, it was found that the best operating temperature of the basic ORC is 300 °C. This cycle was able to enhance the output power by 7.98%. However, this value can increase up to 15.31% when it is replaced by the regenerative ORC. The basic ORC had capital cost and payback period ranges of £11,945–18,770 and 4.9–7.8 years, respectively, while those

Table 8
Final estimates for the basic organic Rankine cycle's capital and operating cost.

Parameter	Value
Organic Rankine cycle (£)	7218–9624
High density polyethylene (£)	1782
Groundwork (£)	2945–7364
Total capital cost (£)	11,945–18,770
Operating cost (£/kWh)	0.173
Diesel consumption (L/kWh)	0.34
Net profit (£/year)	2419
Payback period (years)	4.9–7.8

Table 9
Final estimates for the regenerative organic Rankine cycle's capital and operating cost.

Parameter	Value
Organic Rankine cycle (£)	12,335–16,446
High density polyethylene (£)	1782
Groundwork (£)	2945–7364
Total capital cost (£)	17,062–25,592
Operating cost (£/kWh)	0.168
Diesel consumption (L/kWh)	0.32
Net profit (£/year)	4640
Payback period (years)	3.7–5.5

of the regenerative ORC were £17,062–25,592 and 3.7–5.5 years.

The proposed system was applied to a specific case study (diesel generator) in this paper. However, testing this system on further applications is critical for figuring out the limitations of the system and determining where it can be feasible. The feasibility of using the proposed system in other regions could also be investigated in future studies. This is very crucial since the system is highly affected by the ambient air and ground temperatures, which indeed vary based on the location. This work would encourage the use of shallow geothermal energy systems.

Declaration of Competing Interest

The authors declare that they have no known competing financial interests or personal relationships that could have appeared to influence the work reported in this paper.

Data availability

No data was used for the research described in the article.

References

[1] C. Ononogbo, et al., Opportunities of waste heat recovery from various sources: review of technologies and implementation, Heliyon 9 (2) (2023) e13590, https://doi.org/10.1016/j.heliyon.2023.e13590, 2023/02/01/.

[2] D. Brough, H. Jouhara, The aluminium industry: a review on state-of-the-art technologies, environmental impacts and possibilities for waste heat recovery, Int. J. Thermofluids (2020), 100007, https://doi.org/10.1016/j.ijft.2019.100007, 1-22020/02/01/.

[3] H. El Hage, M. Ramadan, H. Jaber, M. Khaled, A.G. Olabi, A short review on the techniques of waste heat recovery from domestic applications, Energy Sources, Part A: Recovery, Utilization, and Environ. Effects 42 (24) (2020) 3019–3034.

[4] J. Thaddaeus, G.O. Unachukwu, C.A. Mgbemene, A. Pesyridis, M. Usman, F. A. Alshammari, Design, size estimation, and thermodynamic analysis of a realizable organic Rankine cycle system for waste heat recovery in commercial truck engines, Therm. Sci. Eng. Progress 22 (2021), 100849, https://doi.org/10.1016/j.tsep.2021.100849, 2021/05/01/.

[5] M. Venturelli, D. Brough, M. Milani, L. Montorsi, H. Jouhara, Comprehensive numerical model for the analysis of potential heat recovery solutions in a ceramic industry, Int. J. Thermofluids 10 (2021), 100080, https://doi.org/10.1016/j.ijft.2021.100080, 2021/05/01/.

[6] S. Chakraborty, D. Vernon, A. Jha, V. Narayanan, Performance characterization of M-cycle indirect evaporative cooler and heat recovery ventilator for commercial buildings – Experiments and model", Energy Build. 281 (2023), 112762 https://doi.org/10.1016/j.enbuild.2022.112762, 2023/02/15/.

[7] T. Ouyang, P. Qin, X. Tan, J. Wang, J. Fan, A novel peak shaving framework for coal-fired power plant in isolated microgrids: combined flexible energy storage and waste heat recovery, J. Clean. Prod. 374 (2022), 133936, https://doi.org/10.1016/j.jclepro.2022.133936, 2022/11/10/.

[8] H. Jouhara, N. Khordehgah, S. Almahmoud, B. Delpech, A. Chauhan, S.A. Tassou, Waste heat recovery technologies and applications, Therm. Sci. Eng. Progress 6 (2018) 268–289, https://doi.org/10.1016/j.tsep.2018.04.017, 2018/06/01/.

[9] J.J. Fierro, C. Nieto-Londoño, A. Escudero-Atehortua, M. Giraldo, H. Jouhara, L. C. Wrobel, Techno-economic assessment of a rotary kiln shell radiation waste heat recovery system, Therm. Sci. Eng. Progress 23 (2021), 100858, https://doi.org/10.1016/j.tsep.2021.100858, 2021/06/01/.

[10] D. Brough, J. Ramos, B. Delpech, H. Jouhara, Development and validation of a TRNSYS type to simulate heat pipe heat exchangers in transient applications of waste heat recovery, Int. J. Thermofluids 9 (2021), 100056, https://doi.org/10.1016/j.ijft.2020.100056, 2021/02/01/.

[11] A. Kasaeian, et al., Organic Rankine cycles powered by parabolic trough collectors: an overview, Sustain. Energy Technol. Assessments 54 (2022), 102847, https://doi.org/10.1016/j.seta.2022.102847, 2022/12/01/.

[12] M. Javad Dehghani, Enhancing energo-exergo-economic performance of Kalina cycle for low- to high-grade waste heat recovery: design and optimization through deep learning methods, Appl. Therm. Eng. 195 (2021), 117221, https://doi.org/10.1016/j.applthermaleng.2021.117221, 2021/08/01/.

[13] H. Jouhara, et al., Thermoelectric generator (TEG) technologies and applications, Int. J. Thermofluids 9 (2021), 100063, https://doi.org/10.1016/j.ijft.2021.100063, 2021/02/01/.

[14] X. Shanqing, W. Daohong, Design features of air and gas double preheating regenerative burner reheating furnace, Energy Procedia 66 (2015) 189–192, https://doi.org/10.1016/j.egypro.2015.02.015, 2015/01/01/.

[15] C. Wang, et al., Application of a low pressure economizer for waste heat recovery from the exhaust flue gas in a 600 MW power plant, Energy 48 (1) (2012) 196–202, https://doi.org/10.1016/j.energy.2012.01.045, 2012/12/01/.

[16] V.K. Vikraman, P. Subramanian, D.P. Kumar, S. Sriramajayam, R. Mahendiran, S. Ganapathy, Air flowrate and particle size effect on gasification of arecanut husk with preheated air through waste heat recovery from syngas, Bioresource Technol. Reports 17 (2022), 100977, https://doi.org/10.1016/j.biteb.2022.100977, 2022/02/01/.

[17] H. Jouhara, et al., Waste heat recovery solution based on a heat pipe heat exchanger for the aluminium die casting industry, Energy 266 (2023), 126459, https://doi.org/10.1016/j.energy.2022.126459, 2023/03/01/.

[18] M. Mahmoud, et al., Waste heat recovery applications incorporating phase change materials, Encyclopedia of Smart Mater. 2 (2022) 513–521, https://doi.org/10.1016/B978-0-12-815732-9.00074-7, 2022/01/01/.

[19] A.E. Elahi, T. Mahmud, M. Alam, J. Hossain, B.N. Biswas, Exergy analysis of organic Rankine cycle for waste heat recovery using low GWP refrigerants, Int. J. Thermofluids 16 (2022), 100243, https://doi.org/10.1016/j.ijft.2022.100243, 2022/11/01/.

[20] Y.A.A. Laouid, C. Kezrane, Y. Lasbet, A. Pesyridis, Towards improvement of waste heat recovery systems: a multi-objective optimization of different organic Rankine cycle configurations, Int. J. Thermofluids 11 (2021), 100100, https://doi.org/10.1016/j.ijft.2021.100100, 2021/08/01/.

[21] T. Wilberforce, I. Muhammad, Dynamic modelling and analysis of organic rankine cycle power units for the recovery of waste heat from 110kW proton exchange membrane fuel cell system, Int. J. Thermofluids 17 (2023), 100280, https://doi.org/10.1016/j.ijft.2023.100280, 2023/02/01/.

[22] R. Loni, et al., A critical review of power generation using geothermal-driven organic Rankine cycle, Therm. Sci. Eng. Progress 25 (2021), 101028, https://doi.org/10.1016/j.tsep.2021.101028, 2021/10/01/.

[23] Ashwni, A.F. Sherwani, Analysis of solar energy driven organic Rankine cycle-vapor compression refrigeration system, Therm. Sci. Eng. Progress 35 (2022), 101477, https://doi.org/10.1016/j.tsep.2022.101477, 2022/10/01/.

[24] R. Loni, G. Najafi, E. Bellos, F. Rajaee, Z. Said, M. Mazlan, A review of industrial waste heat recovery system for power generation with Organic Rankine Cycle: recent challenges and future outlook, J. Clean. Prod. 287 (2021) 125070, https://doi.org/10.1016/j.jclepro.2020.125070, 2021/03/10/.

[25] J. Oyekale, B. Oreko, Effects of working fluid mixtures on the exergetic sustainability of a solar-biomass organic Rankine cycle power plant, Therm. Sci. Eng. Progress 36 (2022), 101529, https://doi.org/10.1016/j.tsep.2022.101529, 2022/12/01/.

[26] Y.-q. Feng, et al., Experimental comparison of the performance of basic and regenerative organic Rankine cycles, Energy Conversion and Manag. 223 (2020), 113459, https://doi.org/10.1016/j.enconman.2020.113459, 2020/11/01/.

[27] V.B. Hemadri, P.M.V. Subbarao, Thermal integration of reheated organic Rankine cycle (RH-ORC) with gas turbine exhaust for maximum power recovery, Therm. Sci. Eng. Progress 23 (2021), 100876, https://doi.org/10.1016/j.tsep.2021.100876, 2021/06/01/.

[28] A.N.M. Nihaj Uddin Shan, M. Zayed Mostafa, A. Hossain, M. Shadman Sakib, M. Monjurul Ehsan, Thermal assessment and optimization of process fluids in transcritical organic and transcritical CO2 Rankine cycle for waste energy recuperating system, Energy Conversion and Manag.: X 15 (2022), 100258, https://doi.org/10.1016/j.ecmx.2022.100258, 2022/08/01/.

[29] D. Igbong, Energy and exergy-based performance analyses of a combined recompression supercritical carbon dioxide-organic Rankine cycle for waste-heat recovery, Clean. Energy Syst. 3 (2022), 100022, https://doi.org/10.1016/j.cles.2022.100022, 2022/12/01/.

[30] J. Li, Z. Yang, J. Shen, Y. Duan, Enhancement effects of adding internal heat exchanger on dual-pressure evaporation organic Rankine cycle, Energy 265 (2023), 126329, https://doi.org/10.1016/j.energy.2022.126329, 2023/02/15/.

[31] H. Nami, A. Nemati, F. Jabbari Fard, Conventional and advanced exergy analyses of a geothermal driven dual fluid organic Rankine cycle (ORC), Appl. Therm. Eng. 122 (2017) 59–70, https://doi.org/10.1016/j.applthermaleng.2017.05.011, 2017/07/25/.

[32] A. Surendran, S. Seshadri, An ejector based transcritical regenerative series two-stage organic Rankine cycle for dual/multi-source heat recovery applications, Therm. Sci. Eng. Progress 27 (2022), 101158, https://doi.org/10.1016/j.tsep.2021.101158, 2022/01/01/.

[33] R. Vidhi, D.Y. Goswami, and E. Stefanakos, "Supercritical rankine cycle coupled with ground cooling for low temperature power generation", Energy Procedia, vol. 57, pp. 524–532, 2014/01/01/ 2014, doi: https://doi.org/10.1016/j.egypro.2014.10.206.

[34] M. Mahmoud, M. Ramadan, S. Naher, K. Pullen, A.-.G. Olabi, CO2 – Based transcritical Rankine cycle coupled with a ground-cooled condenser, Therm. Sci.

Eng. Progress 25 (2021), 100948, https://doi.org/10.1016/j.tsep.2021.100948, 2021/10/01/.

[35] M. Mahmoud, M. Alkhedher, M. Ramadan, S. Naher, K. Pullen, An investigation on organic Rankine cycle incorporating a ground-cooled condenser: working fluid selection and regeneration, Energy 249 (2022), 123742, https://doi.org/10.1016/j.energy.2022.123742, 2022/06/15/.

[36] M. Mahmoud, M. Alkhedher, M. Ramadan, K. Pullen, A.-.G. Olabi, S. Naher, Experimental investigation into the potential of using a shallow ground-cooled condenser in Lebanon, Energy Conversion and Manag. 264 (2022), 115729, https://doi.org/10.1016/j.enconman.2022.115729, 2022/07/15/.

[37] C. Yang, et al., Thermal conductivity enhancement of recycled high density polyethylene as a storage media for latent heat thermal energy storage, Solar Energy Mater. Solar Cells 152 (2016) 103–110, https://doi.org/10.1016/j.solmat.2016.02.022, 2016/08/01/.

[38] "HIGH DENSITY POLYETHYLENE - MOL." https://mol.hu/ (accessed March 22, 2023).

[39] "RT21HC - Rubitherm GmbH". https://www.rubitherm.eu/, (accessed March 22, 2023).

[40] R.C. Hibbeler, Mechanics of Materials, Pearson Educación, 2005.

[41] M. Mahmoud, M. Ramadan, S. Naher, K. Pullen, A.-.G. Olabi, Advances in Grout materials in borehole heat exchangers, Encyclopedia of Smart Mater. 4 (2022) 334–342, https://doi.org/10.1016/B978-0-12-815732-9.00053-X, 2022/01/01/.

[42] M. Mahmoud, et al., A review of grout materials in geothermal energy applications, Int. J. Thermofluids 10 (2021), 100070, https://doi.org/10.1016/j.ijft.2021.100070, 2021/05/01/.

[43] F. Chen, J. Mao, S. Chen, C. Li, P. Hou, L. Liao, Efficiency analysis of utilizing phase change materials as grout for a vertical U-tube heat exchanger coupled ground source heat pump system, Appl. Therm. Eng. 130 (2018) 698–709, https://doi.org/10.1016/j.applthermaleng.2017.11.062, 2018/02/05/.

[44] A. Aljabr, A. Chiasson, A. Alhajjaji, Numerical modeling of the effects of micro-encapsulated phase change materials intermixed with grout in vertical borehole heat exchangers, Geothermics 96 (2021), 102197, https://doi.org/10.1016/j.geothermics.2021.102197, 2021/11/01/.

[45] J. Pássaro, A. Rebola, L. Coelho, J. Conde, Numeric study of geothermal borehole heat exchanger enhancement via phase change material macro encapsulation, Int. J. Thermofluids 16 (2022), 100245, https://doi.org/10.1016/j.ijft.2022.100245, 2022/11/01/.

[46] M. Mahmoud et al., "Using nanoparticles for thermal enhancement of phase change materials", Encyclopedia of Smart Mater. vol. 3, pp. 281–287, 2022/01/01/ 2022, https://doi.org/10.1016/B978-0-12-815732-9.00111-X.

[47] H.M. Maghrabie, et al., Phase change materials based on nanoparticles for enhancing the performance of solar photovoltaic panels: a review, J. Energy Storage 48 (2022), 103937, https://doi.org/10.1016/j.est.2021.103937, 2022/04/01/.

[48] M.K. Paliwal, S. Jakhar, V. Sharma, Nano-enhanced phase change materials for energy storage in photovoltaic thermal management systems: a bibliometric and thematic analysis, Int. J. Thermofluids 17 (2023), 100310, https://doi.org/10.1016/j.ijft.2023.100310, 2023/02/01/.

[49] G.K. Amudhalapalli, J.K. Devanuri, Synthesis, characterization, thermophysical properties, stability and applications of nanoparticle enhanced phase change materials – A comprehensive review, Therm. Sci. Eng. Progress 28 (2022), 101049, https://doi.org/10.1016/j.tsep.2021.101049, 2022/02/01/.

[50] M. Mahmoud, et al., Foam-based composite phase change materials, Encyclopedia of Smart Mater. 4 (2022) 343–351, https://doi.org/10.1016/B978-0-12-815732-9.00083-8, 2022/01/01/.

[51] M. Aramesh, B. Shabani, Metal foam-phase change material composites for thermal energy storage: a review of performance parameters, Renew. Sustain. Energy Rev. 155 (2022), 111919, https://doi.org/10.1016/j.rser.2021.111919, 2022/03/01/.

[52] Z. Sun, et al., Experimental study of battery passive thermal management system using copper foam-based phase change materials, Int. J. Thermofluids 17 (2023), 100255, https://doi.org/10.1016/j.ijft.2022.100255, 2023/02/01/.

[53] Y. Sheikh, M.F. Orhan, A. Azmeer, Melting performance of a composite bio-based phase change material: an experimental evaluation of copper foam pore size, Int. J. Thermofluids 16 (2022), 100216, https://doi.org/10.1016/j.ijft.2022.100216, 2022/11/01/.

[54] Y. Sheikh, M.F. Orhan, M. Umair, E. Mehaisi, A. Azmeer, Variation in cooling performance of a bio-based phase change material by adding graphene nanoplatelets with surfactants, Int. J. Thermofluids 16 (2022), 100201, https://doi.org/10.1016/j.ijft.2022.100201, 2022/11/01/.

[55] O. Okogeri, V.N. Stathopoulos, What about greener phase change materials? A review on biobased phase change materials for thermal energy storage applications", Int. J. Thermofluids 10 (2021), 100081 https://doi.org/10.1016/j.ijft.2021.100081, 2021/05/01/.

[56] Z. Qiu, X. Ma, P. Li, X. Zhao, A. Wright, Micro-encapsulated phase change material (MPCM) slurries: characterization and building applications, Renew. Sustain. Energy Rev. 77 (2017) 246–262, https://doi.org/10.1016/j.rser.2017.04.001, 2017/09/01/.

[57] Z. Fu, et al., Experimental investigation on the enhanced performance of a solar PVT system using micro-encapsulated PCMs, Energy 228 (2021), 120509, https://doi.org/10.1016/j.energy.2021.120509, 2021/08/01/.

[58] J. Rostami, Convective heat transfer by micro-encapsulated PCM in a mini-duct, Int. J. Therm. Sci. 161 (2021), 106737, https://doi.org/10.1016/j.ijthermalsci.2020.106737, 2021/03/01/.

[59] K. Faraj, M. Khaled, J. Faraj, F. Hachem, K. Chahine, C. Castelain, Energetic and economic analyses of integrating enhanced macro-encapsulated PCM's with active underfloor hydronic heating system, Energy Reports 8 (2022) 848–862, https://doi.org/10.1016/j.egyr.2022.07.099, 2022/11/01/.

[60] E. Mohseni, W. Tang, S. Wang, Development of thermal energy storage lightweight structural cementitious composites by means of macro-encapsulated PCM, Construction and Build. Mater. 225 (2019) 182–195, https://doi.org/10.1016/j.conbuildmat.2019.07.136, 2019/11/20/.

[61] A.K. Raj, M. Srinivas, S. Jayaraj, A cost-effective method to improve the performance of solar air heaters using discrete macro-encapsulated PCM capsules for drying applications, Appl. Therm. Eng. 146 (2019) 910–920, https://doi.org/10.1016/j.applthermaleng.2018.10.055, 2019/01/05/.

[62] L. Tocci, T. Pal, I. Pesmazoglou, B. Franchetti, Small scale organic rankine cycle (ORC): a techno-economic review, Energies 10 (4) (2017) 413.